In situ creation and tailoring of interfacial quantum dots in graphene/transition metal dichalcogenide heterostructures

Ya-Ning Ren,[*] Mo-Han Zhang,[*] Xiao-Feng Zhou,[*] Qi Zheng ,[*] Hui-Ying Ren, and Lin He [†]

Center for Advanced Quantum Studies, School of Physics and Astronomy, Beijing Normal University, Beijing 100875, China
and Key Laboratory of Multiscale Spin Physics, Ministry of Education, Beijing 100875, China

Control of doping and carrier concentration at the nanoscale is an essential requirement to realize future electronic and optoelectronic devices in two-dimensional van der Waals (vdW) heterostructures. In spite of great efforts on the related study, introducing nanoscale high-quality junctions with custom-designed sizes and sites remains an outstanding challenge in experiments. Here, we overcome the challenges by combining scanning tunneling microscope (STM) lithography with structural phase transition of transition metal dichalcogenides (TMDs). Our experiments demonstrate that nanoscale TMD islands can be created, moved, sliced, and merged at the interface of graphene/TMD heterostructures by using a STM tip. The reported method can *in situ* introduce the structural phase transition in the interfacial TMD islands, generating well-defined nanoscale electrostatic potentials in graphene and enabling the realization of custom-designed artificial model systems. Our result enables the creation of high-quality patterned quantum confined systems to fully engineer electronic and optoelectronic properties of vdW heterostructures.

I. INTRODUCTION

Introducing high-quality electronic potentials in two-dimensional (2D) materials is vital to explore exotic phenomena predicted in fundamental physics. Notable examples are the realization of the Klein tunneling and atomic collapse states in graphene with well-defined electronic potentials [1–18]. Besides that, patterning high-quality electronic potentials in 2D materials is a powerful method to tune the band structures and control behaviors of charge carriers [19–22]. Therefore, it is also an essential requirement to realize nanoscale electronic and optoelectronic devices with tunable properties [23–29], which has long been a pursuit of the material science community. During the past 10 years, several different strategies have been developed to introduce electronic potentials in 2D materials [5–18,26–29]. However, realizing nanoscale high-quality electronic potentials with well-defined sizes and sites in 2D materials is still an extreme challenge in experiment up to now. Here we overcome this challenge and report a route to realize patterns of nanoscale high-quality electronic potentials with custom-designed sizes and positions in graphene/transition metal dichalcogenide (TMD) heterostructures. By using scanning tunneling microscope (STM) lithography [30–32], we create monolayer TMD islands with tunable sizes and sites at the interfaces of four different graphene/TMD heterostructures. The interfacial TMD islands undergo a structural phase transition [33,34], thereby introducing well-defined electrostatic potentials on graphene that effectively form graphene quantum dots (QDs), enabling

us to fully engineer the electronic structure of the heterostructures. The reported method helps us to realize a wide variety of high-quality mixed-dimensional heterostructures [35,36] by integration of 2D heterostructures with zero-dimensional QDs.

II. RESULTS AND DISCUSSION

In our experiment, four different high-quality graphene/TMD heterostructures are obtained by using transfer technology, as reported previously [15,17,37,38], of graphene monolayer onto mechanically exfoliated TMD sheets, including WSe_2, WS_2, $MoSe_2$, and $MoTe_2$. Here we show that we can create interfacial islands in the graphene/TMD heterostructures through voltage pulses applied to the STM tip, as schematically shown in Figs. 1(a)–1(c). By using a STM tip with a large voltage pulse (see Fig. S1 in the Supplemental Material [39] as an example), our experiment indicates that the supporting TMD substrate can be locally fractured even though it is covered with graphene. Then, nanoscale pits are generated in the substrates and we are able to "create" interfacial monolayer/bilayer TMD islands from the pits in the substrates. Figure 1(d) shows a representative STM image of a monolayer WSe_2 island generated at the interface of graphene/WSe_2 heterostructure and the thickness of the island is the same as that of a WSe_2 monolayer $\sim$0.8–1.0 nm. In our experiment, nanoscale pits of the bulk TMD substrates are usually observed around the interfacial TMD islands (see Figs. S2–S4 in the Supplemental Material [39]), further confirming that the interfacial TMD islands are generated from the pits of the substrate. The topmost graphene monolayer is unattacked by the tip pulses and there is no graphene fragment around the WSe_2 pits and islands.

---

[*]These authors contributed equally to this work.
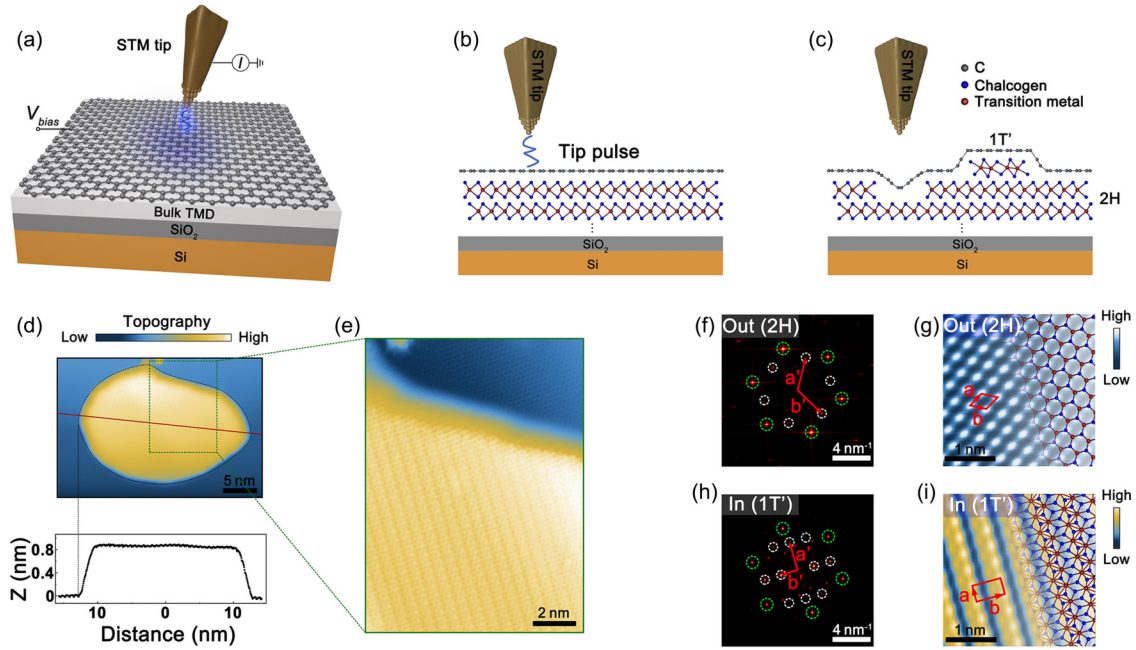[†]Contact author: helin@bnu.edu.cn

FIG. 1. *In situ* creating interfacial TMD islands in graphene/TMD heterostructures. (a) Sketch of the STM setup. (b) and (c) Schematics of graphene/TMD heterostructures before and after an applied tip pulse, respectively. (d) Top: The STM image ($V_b = 350$ mV, $I = 400$ pA) of a graphene/WSe$_2$ heterostructure QD. Bottom: A height profile across the WSe$_2$ island. (e) Atomic-resolved STM image. (f) and (h) Fast Fourier transform (FFT) images obtained from the STM image off and on the QD, respectively. The green and white circles show reciprocal lattices of graphene and WSe$_2$, respectively. The unlabeled bright spots correspond to the reciprocal moiré superlattices and higher-order scattering. (g) and (i) Inverse FFT images obtained by filtering the components of WSe$_2$ lattices off and on the QD, respectively.

Such a result is quite reasonable because the C-C bond in graphene is rather strong, and the fracture stress of graphene is about six times larger than that of WSe$_2$ [40].

One key observation in our experiment is that there is a structural phase transition in the interfacial TMD islands. Here we still introduce the result of graphene/WSe$_2$ heterostructure as an example and the results obtained in other graphene/TMD heterostructures are similar. Although the WSe$_2$ islands are covered by a graphene sheet, it is still possible to obtain their atomic-resolved STM images. The WSe$_2$ substrate is characterized by a trigonal-prismatic coordination of transition metal atoms and it is denoted as the $1H$ ($2H$) phase in the single-layer (bulk) form, as shown in Figs. 1(f) and 1(g). However, the interfacial WSe$_2$ islands become monoclinic $1T'$ phase after the tip pulse, as shown in Figs. 1(e), 1(h), and 1(i). Then, the adjacent two tungsten arrays become closer to each other, making one array of top Se atoms become higher than the adjacent array, which can be clearly observed in the STM measurements. According to previous studies [33,34], the mechanical strain, the electronic doping, the atomic defects, and so on can result in the structural transition from the $1H$ phase to the $1T'$ phase of the TMDs. Therefore, the strain induced by the adjacent graphene and WSe$_2$ substrate during the fractured process, local electrostatic gating induced by the STM tip, and edge atoms of the interfacial WSe$_2$ islands may induce the observed structural phase transition. Although many different methods have been developed to introduce the structural phase transitions in the TMDs [33,34], the reported result here is quite unique because it provides an unprecedented

opportunity to *in situ* introduce the structural phase transition at custom-designed sites and with nanoscale precision. Moreover, by presetting the coordinates of the STM tip and using a series of voltage pulses, then, different custom-designed patterns of the islands can be obtained (see Supplemental Material [39] Fig. S5).

The other key observation in this work is that all the interfacial TMD islands can introduce electrostatic potentials on the graphene above them, generating quasibound states in graphene, which effectively form graphene QDs (see Supplemental Material [39] Figs. S6–S8). To explore the origin of this, we measured atomic structures of hundreds of the interfacial TMD islands and studied the electronic properties of graphene above them. Our experiments demonstrate that the induced local electrostatic potential in graphene is closely related to the structural phase transition of the TMD islands. Here we still introduce the result of graphene/WSe$_2$ heterostructure as an example, as summarized in Fig. 2. In our experiment, most of the interfacial WSe$_2$ islands become monoclinic $1T'$ phase after the tip pulse, with only a few of the studied interfacial WSe$_2$ nanostructures remaining in the $1H$ phase. Figure 2(a) shows a representative STM image of two interfacial WSe$_2$ islands in the heterostructure: one is in the $1T''$phase and the other is in the $1H$ phase. The atomic-resolved STM characterizations of the two interfacial WSe$_2$ islands covered by graphene are summarized in Figs. 2(c)–2(h). Figure 2(b) shows typical scanning tunneling spectroscopy (STS) spectra measured in the graphene on and off the WSe$_2$ islands and Fig. 2(i) shows represen-
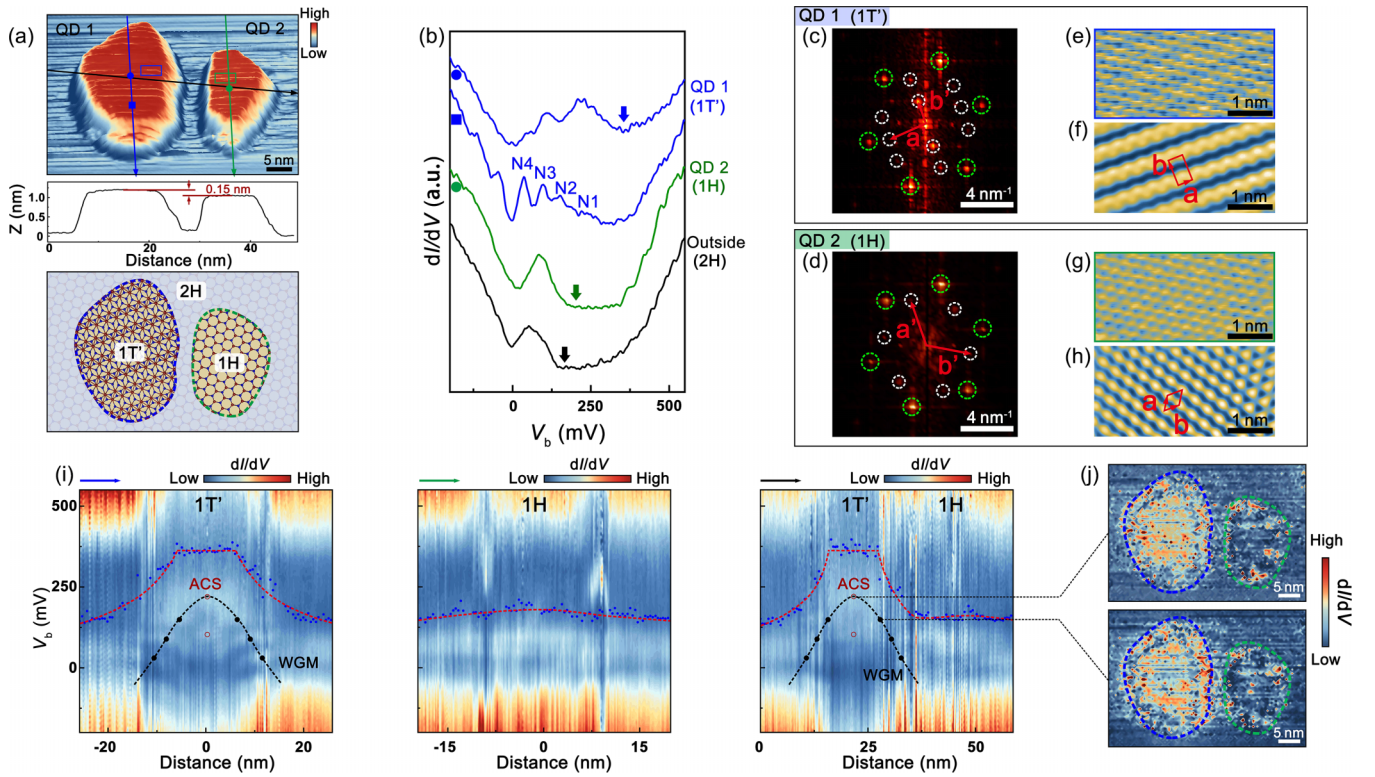
FIG. 2. (a) A STM image ($V_b = 500$ mV, $I = 200$ pA) of two graphene/WSe$_2$ heterostructure QDs. QD 1 (QD 2) is the graphene-covered $1T'$-phase ($1H$-phase) WSe$_2$ island. Middle: The height profile of QD 1 and QD 2. Bottom: Schematics of graphene/TMD heterostructure with two interfacial islands. (b) Typical dI/dV spectra measured off (black line) and on the QD 1 (blue lines) and QD 2 (green line) in panel (a). The arrows denote the positions of the Dirac points. (c) and (d) The FFT images obtained from STM images on QD 1 and QD 2, respectively. The green and white circles show the reciprocal lattices of graphene and WSe$_2$, respectively. The red arrows show the reciprocal lattice vectors a' and b' of WSe$_2$. (e) and (g). Enlarged STM images ($V_b = 500$ mV, $I = 200$ pA) of QD 1 and QD 2, respectively. (f) and (h) Reverse FFT by filtering the components of WSe$_2$ lattices in the white circles in panels (c) and (d), respectively. Red rectangle and rhombus depict the unit cells of $1T'$ and $1H$ WSe$_2$, respectively (with unit vectors a and b). (i) The dI/dV spectroscopic maps measured along the direction of different colored solid lines in panel (a). The blue solid dots indicate the Dirac point. The red dashed lines are guides to the eye. (j) STS maps recorded at different energies around the graphene/WSe$_2$ heterostructure QDs.

tative STS, i.e., dI/dV, spectroscopic maps recorded across the graphene/WSe$_2$ heterostructure QDs. For the graphene covering the $1T'$-phase WSe$_2$ island, the supporting substrates of graphene on and off the QD are the $1T'$-phase and $2H$-phase WSe$_2$, respectively, which have quite different electronic properties and work functions [33,34]. Then, we observe large variations of the local doping in graphene on and off the $1T'$-phase WSe$_2$ islands and a sequence of temporarily confined quasibound states, shown as resonance peaks in the spectrum, are clearly observed [see Fig. 2(b) and the left panel of Fig. 2(i)]. According to the measured spatial-dependent Dirac points [Fig. 2(i)], the $1T'$ WSe$_2$ island introduces Coulomb-like electrostatic potential on the graphene above it, which generates both atomic collapse states (ACSs) and whispering gallery modes (WGMs) in graphene [15,17]. The ACSs locate at the center of the potential field due to collapse by the Coulomb potential, while the WGMs locate at the edge of the potential profile due to the large cut-off radius of the Coulomb potential [15,17]. Both the ACSs and the WGMs can be directly imaged in STS maps at selected energies, as shown in Fig. 2(j). The slight spa-

tial dispersion of the quasibound states observed in the STS linecuts is mainly due to the STM tip potential distorting the potential. For the graphene covering the $1H$-phase WSe$_2$ island, both the supporting substrates of graphene on and off the QD are the H-phase WSe$_2$. In this case, we only observe a very small variation of the local doping [see Fig. 2(b), middle and right panels of Fig. 2(i)], which may arise from effects of dangling bonds at the edge of the island, and it is difficult to observe a series of quasibound states (see Supplemental Material [39] Fig. S9 for more experimental data).

The cut-off shape of the electrostatic potential plays a vital role in determining the electronic properties of the graphene QDs [15,17]. According to our experiment, the cut-off shape of the Coulomb potential is mainly determined by the geometry of the interfacial TMD islands [see Fig. 2(i) and Supplemental Material [39] Figs. S6–S8]. Below, we will show that the interfacial TMD islands can be moved, sliced, and merged with an STM tip (as summarized in Figs. 3 and 4), which provides an unprecedented opportunity to *in situ* tune the electrostatic potentials in the heterostructures. By moving
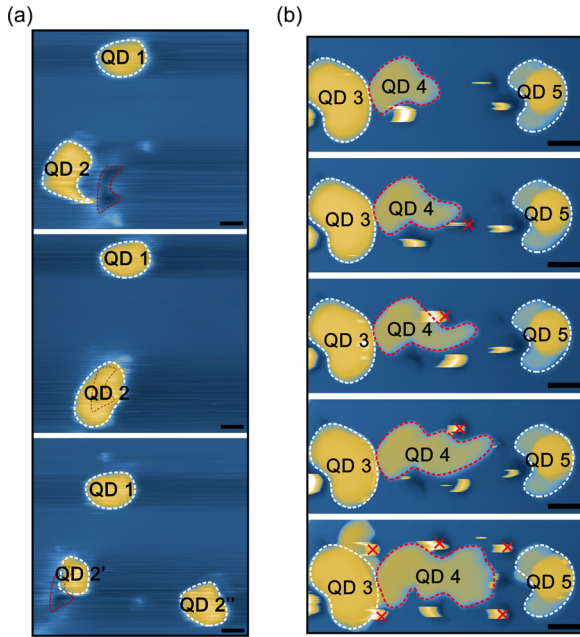
FIG. 3. (a) A representative result of tailoring the interfacial WSe$_2$ islands. QD 2 is first moved to a nearby pit of the WSe$_2$ substrate. Then, it is tailored into two pieces, QD 2′ and QD 2″, when it is lifted by the STM tip. The scale bar is 10 nm. (b) The area of the WSe$_2$ QD 4 increases with increasing the number of tip pulses (the positions that applied the tip pulses are marked by "×"). The scale bar is 5 nm.

the STM tip along a given direction, the WSe$_2$ islands can be moved to a selected position even though they are buried at the interface of the graphene/WSe$_2$ heterostructures. We demonstrate the ability to tune the positions of the interfacial WSe$_2$ islands with nanoscale precision, as shown in Fig. 4 (see Supplemental Material [39] Fig. S10 for more experimental data). Because of the small fracture stress of WSe$_2$, we further show the ability to slice the interfacial islands by using the STM tip. Figure 3(a) shows a typical result. First, the selected WSe$_2$ island is moved to a nearby pit of the WSe$_2$ substrate. The edge atoms of the pit seem to increase the interaction between the WSe$_2$ island and the WSe$_2$ substrate. Then, by moving the STM tip, the WSe$_2$ island can be sliced into two pieces. Our experiment further demonstrates that the area of the interfacial WSe$_2$ island can be continuously tuned by merging the smaller WSe$_2$ fragments from the pit of the substrate. To confirm this, several tip pulses are applied around an interfacial WSe$_2$ island, as shown in Fig. 3(b). With increasing the number of tip pulses, the area of the adjacent single-crystal WSe$_2$ island increases. Such a result demonstrates explicitly that the small WSe$_2$ fragments at the interface will be merged into a larger single-crystal WSe$_2$ island, which implies that the local Joule heating generated by the tip pulse plays an important role in the merging process. This result also helps

us to understand the result that the area of the interfacial WSe$_2$ island is usually several times larger than that of the corresponding nearby WSe$_2$ pit (see Supplemental Material [39] Fig. S11 for details and more discussion).

Combining the ability to tune the positions and tailor the sizes of the interfacial islands, the method reported here may open an avenue to build custom-designed patterns of the WSe$_2$ islands to realize artificial model systems via coupled quasibound states in graphene. Figure 4 shows the simplest example realized in our experiment: the distance ΔD, i.e., the tunneling coupling, between two graphene/WSe$_2$ heterostructure QDs is continuously tuned. For the case that $\Delta D \approx$ 80 nm, the tunneling coupling between the two graphene QDs is very weak and the two graphene QDs can be regarded as two isolated QDs. Because of the similar sizes of the two QDs, they exhibit almost identical quasibound states, as shown in Fig. 4(f), and the energy separations between the quasibound states are almost the same. Outside the QDs, interference features of the massless Dirac fermions can be clearly identified. By decreasing the distance, the averaged energy separation between the quasibound states of the two QDs decreases slightly due to the slight overlapping of their electrostatic potentials (consequently, the effective confined size of the quasibound states increases). When the distance is decreased to $\Delta D \approx$ 30 nm, as shown in Fig. 4(j), the quasibound states of the two QDs are strongly hybridized, and they become delocalized over both QDs. Such a process with custom-designed coupling reveals a process in the formation of coupled QDs with decreasing the distance between the two QDs.

III. CONCLUSIONS

In summary, we report a universal method in patterning of TMD islands with nanometer-precision, tunable sizes and sites at the interfaces of graphene/TMD heterostructures. The reported method helps us to realize a wide variety of high-quality mixed-dimensional heterostructures, which opens an avenue to fully engineer the electronic structure of the heterostructures and can help us to realize custom-designed artificial model systems.
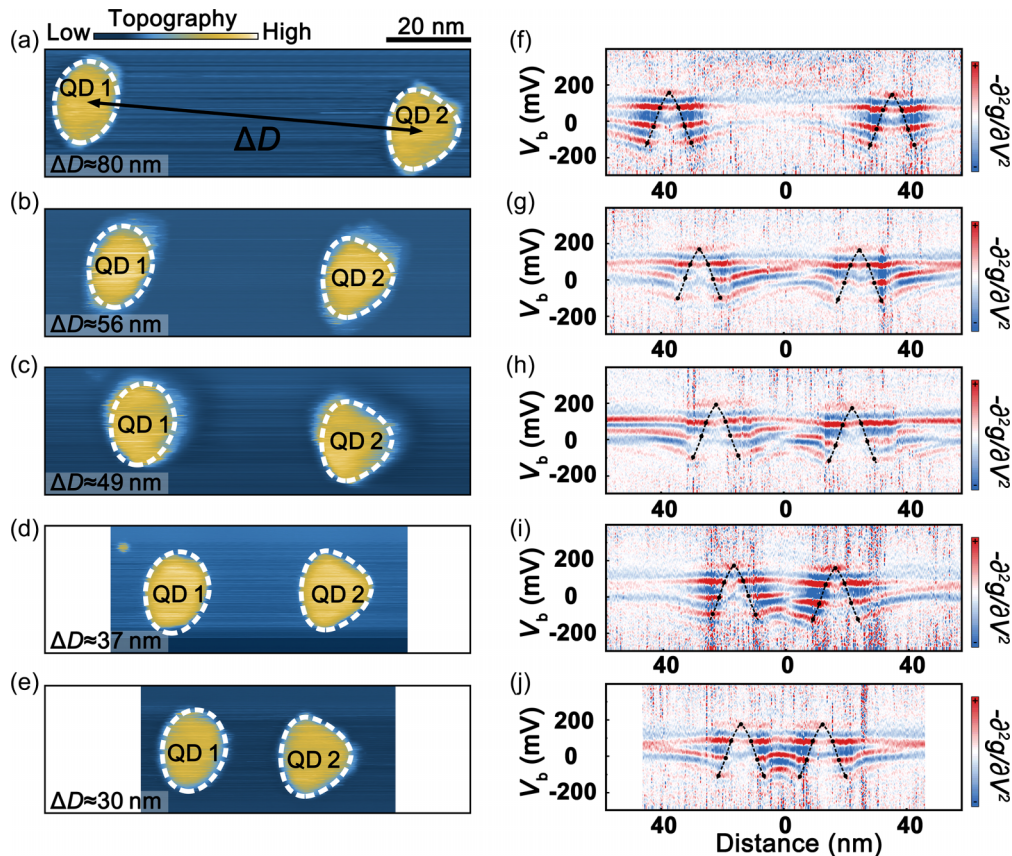
ACKNOWLEDGMENTS

FIG. 4. (a)–(e) STM images of two graphene/WSe$_2$ heterostructure QDs with different distances ΔD. By moving the STM tip in a specified direction, the interfacial WSe$_2$ islands can be brought closer together. (f)–(j) Spectroscopic maps measured crossing the centers of the graphene/WSe$_2$ heterostructure QDs. Here, $g = dI/dV$ reflects the local density of states around the QDs. The negative second derivative of dI/dV is used to enhance the visibility of the peak positions. The black solid dots indicate the quasibound states via the WGMs confinement. At $\Delta D \approx 80$ nm, the quantum dots behave as nearly isolated entities with minimal coupling. As the distance decreases to 30 nm $< \Delta D \leqslant 56$ nm, overlapping electrostatic potentials enhance Coulomb interaction, leading to anticrossing behavior where one QD's states are lifted and the other's are lowered. At $\Delta D \approx 30$ nm, the quasibound states hybridize into bonding and antibonding orbitals, becoming delocalized across both QDs, reducing Coulomb interaction.

[1] M. I. Katsnelson, K. S. Novoselov, and A. K. Geim, Chiral tunnelling and the Klein paradox in graphene, Nat. Phys. **2**, 620 (2006).

[2] V. M. Pereira, J. Nilsson, and A. H. Castro Neto, Coulomb impurity problem in graphene, Phys. Rev. Lett. **99**, 166802 (2007).

[3] A. V. Shytov, M. I. Katsnelson, and L. S. Levitov, Vacuum polarization and screening of supercritical impurities in graphene, Phys. Rev. Lett. **99**, 236801 (2007).

[4] A. V. Shytov, M. I. Katsnelson, and L. S. Levitov, Atomic collapse and quasi-Rydberg states in graphene, Phys. Rev. Lett. **99**, 246802 (2007).

[5] Y. Zhao, J. Wyrick, F. D. Natterer, J. F. Rodriguez-Nieva, C. Lewandowski, K. Watanabe, T. Taniguchi, L. S. Levitov, N. B. Zhitenev, and J. A. Stroscio, Creating and probing electron whispering-gallery modes in graphene, Science **348**, 672 (2015).

[6] C. Gutiérrez, L. Brown, C.-J. Kim, J. Park, and A. N. Pasupathy, Klein tunnelling and electron trapping in nanometre-scale graphene quantum dots, Nat. Phys. **12**, 1069 (2016).

[7] J. Lee, D. Wong, J. Velasco Jr., J. F. Rodriguez-Nieva, S. Kahn, H.-Z. Tsai, T. Taniguchi, K. Watanabe, A. Zettl, and F. Wang, Imaging electrostatically confined Dirac fermions in graphene quantum dots, Nat. Phys. **12**, 1032 (2016).

[8] K.-K. Bai, J.-J. Zhou, Y.-C. Wei, J.-B. Qiao, Y.-W. Liu, H.-W. Liu, H. Jiang, and L. He, Generating atomically sharp $p-n$ junctions in graphene and testing quantum electron optics on the nanoscale, Phys. Rev. B **97**, 045413 (2018).

[9] Z.-Q. Fu, K.-K. Bai, Y.-N. Ren, J.-J. Zhou, and L. He, Coulomb interaction in quasibound states of graphene quantum dots, Phys. Rev. B **101**, 235310 (2020).

[10] Z.-Q. Fu, Y. Pan, J.-J. Zhou, K.-K. Bai, D.-L. Ma, Y. Zhang, J.-B. Qiao, H. Jiang, H. Liu, and L. He, Relativistic artificial

molecules realized by two coupled graphene quantum dots, Nano Lett. **20**, 6738 (2020).

[11] F. Ghahari, D. Walkup, C. Gutiérrez, J. F. Rodriguez-Nieva, Y. Zhao, J. Wyrick, F. D. Natterer, W. G. Cullen, K. Watanabe, T. Taniguchi *et al.*, An on/off Berry phase switch in circular graphene resonators, Science **356**, 845 (2017).

[12] Y. Wang, D. Wong, A. V. Shytov, V. W. Brar, S. Choi, Q. Wu, H.-Z. Tsai, W. Regan, A. Zettl, R. K. Kawakami *et al.*, Observing atomic collapse resonances in artificial nuclei on graphene, Science **340**, 734 (2013).

[13] J. Mao, Y. Jiang, D. Moldovan, G. Li, K. Watanabe, T. Taniguchi, M. R. Masir, F. M. Peeters, and E. Y. Andrei, Realization of a tunable artificial atom at a supercritically charged vacancy in graphene, Nat. Phys. **12**, 545 (2016).

[14] Y. Jiang, J. Mao, D. Moldovan, M. R. Masir, G. Li, K. Watanabe, T. Taniguchi, F. M. Peeters, and E. Y. Andrei, Tuning a circular *p-n* junction in graphene from quantum confinement to optical guiding, Nat. Nanotechnol. **12**, 1045 (2017).

[15] Q. Zheng, Y.-C. Zhuang, Q.-F. Sun, and L. He, Coexistence of electron whispering-gallery modes and atomic collapse states in graphene/WSe$_2$ heterostructure quantum dots, Nat. Commun. **13**, 1597 (2022).

[16] Y.-N. Ren, Q. Cheng, Q.-F. Sun, and L. He, Realizing valley-polarized energy spectra in bilayer graphene QDs via continuously tunable Berry phases, Phys. Rev. Lett. **128**, 206805 (2022).

[17] Q. Zheng, Y.-C. Zhuang, Y.-N. Ren, C. Yan, Q.-F. Sun, L. He *et al.*, Molecular collapse states in graphene/WSe$_2$ heterostructure quantum dots, Phys. Rev. Lett. **130**, 076202 (2023).

[18] Z. Ge, S. Slizovskiy, P. Polizogopoulos, T. Joshi, T. Taniguchi, K. Watanabe, D. Lederman, V. I. Fal'ko, and J. Velasco, Giant orbital magnetic moments and paramagnetic shift in artificial relativistic atoms and molecules, Nat. Nanotechnol. **18**, 250 (2023).

[19] S. Chen, Z. Han, M. M. Elahi, K. M. Habib, L. Wang, B. Wen, Y. Gao, T. Taniguchi, K. Watanabe, and J. Hone, Electron optics with *p-n* junctions in ballistic graphene, Science **353**, 1522 (2016).

[20] V. V. Cheianov, V. Fal'ko, and B. L. Altshuler, The focusing of electron flow and a Veselago lens in graphene *p-n* junctions, Science **315**, 1252 (2007).

[21] C.-H. Park, L. Yang, Y.-W. Son, M. L. Cohen, and S. G. Louie, New generation of massless Dirac fermions in graphene under external periodic potentials, Phys. Rev. Lett. **101**, 126804 (2008).

[22] C.-H. Park, L. Yang, Y.-W. Son, M. L. Cohen, and S. G. Louie, Anisotropic behaviours of massless Dirac fermions in graphene under periodic potentials, Nat. Phys. **4**, 213 (2008).

[23] J. F. Sierra, J. Fabian, R. K. Kawakami, S. Roche, and S. O. Valenzuela, Van der Waals heterostructures for spintronics and opto-spintronics, Nat. Nanotechnol. **16**, 856 (2021).

[24] K. S. Novoselov, A. Mishchenko, A. Carvalho, and A. H. Castro Neto, 2D materials and van der Waals heterostructures, Science **353**, aac9439 (2016).

[25] W. J. Yu, Y. Liu, H. Zhou, A. Yin, Z. Li, Y. Huang, and X. Duan, Highly efficient gate-tunable photocurrent generation in vertical heterostructures of layered materials, Nat. Nanotechnol. **8**, 952 (2013).

[26] B. W. H. Baugher, H. O. H. Churchill, Y. Yang, and P. Jarillo-Herrero, Optoelectronic devices based on electrically tunable *p-n* diodes in a monolayer dichalcogenide, Nat. Nanotechnol. **9**, 262 (2014).

[27] A. Pospischil, M. M. Furchi, and T. Mueller, Solar-energy conversion and light emission in an atomic monolayer *p-n* diode, Nat. Nanotechnol. **9**, 257 (2014).

[28] J. S. Ross, P. Klement, A. M. Jones, N. J. Ghimire, J. Yan, D. G. Mandrus, T. Taniguchi, K. Watanabe, K. Kitamura, W. Yao *et al.*, Electrically tunable excitonic light-emitting diodes based on monolayer WSe$_2$ *p-n* junctions, Nat. Nanotechnol. **9**, 268 (2014).

[29] C.-H. Lee, G.-H. Lee, A. M. van der Zande, W. Chen, Y. Li, M. Han, X. Cui, G. Arefe, C. Nuckolls, T. F. Heinz *et al.*, Atomically thin *p-n* junctions with van der Waals heterointerfaces, Nat. Nanotechnol. **9**, 676 (2014).

[30] L. Tapasztó, G. Dobrik, P. Lambin, and L. P. Biró, Tailoring the atomic structure of graphene nanoribbons by scanning tunnelling microscope lithography, Nat. Nanotechnol. **3**, 397 (2008).

[31] G. Z. Magda, X. Jin, I. Hagymási, P. Vancsó, Z. Osváth, P. Nemes-Incze, C. Hwang, L. P. Biró, and L. Tapasztó, Room-temperature magnetic order on zigzag edges of narrow graphene nanoribbons, Nature (London) **514**, 608 (2014).

[32] P. Jia, W. Chen, J. Qiao, M. Zhang, X. Zheng, Z. Xue, R. Liang, C. Tian, L. He, Z. Di, and X. Wang, Programmable graphene nanobubbles with three-fold symmetric pseudo-magnetic fields, Nat. Commun. **10**, 3127 (2019).

[33] H. Yang, S. W. Kim, M. Chhowalla, and Y. H. Lee, Structural and quantum-state phase transitions in van der Waals layered materials, Nat. Phys. **13**, 931 (2017).

[34] X. Yin, C. S. Tang, Y. Zheng, J. Gao, J. Wu, H. Zhang, M. Chhowalla, W. Chen, and A. T. S. Wee, Recent developments in 2D transition metal dichalcogenides: Phase transition and applications of the (quasi-)metallic phases, Chem. Soc. Rev. **50**, 10087 (2021).

[35] D. Jariwala, T. J. Marks, and M. C. Hersam, Mixed-dimensional van der Waals heterostructures, Nat. Mater. **16**, 170 (2017).

[36] Y. Liu, Y. Huang, and X. Duan, Van der Waals integration before and beyond two-dimensional materials, Nature (London) **567**, 323 (2019).

[37] Y.-X. Zhao, X.-F. Zhou, Y. Zhang, and L. He, Oscillations of van Hove singularities spacing induced by sub-Ångstrom fluctuations of interlayer spacing in graphene superlattices, Phys. Rev. Lett. **127**, 266801 (2021).

[38] Q. Zheng, C.-Y. Hao, X.-F. Zhou, Y.-X. Zhao, J.-Q. He, and L. He, Tunable sample-wide electronic kagome lattice in low-angle twisted bilayer graphene, Phys. Rev. Lett. **129**, 076803 (2022).

[39] See Supplemental Material at http://link.aps.org/supplemental/10.1103/PhysRevB.110.125416 for details on sample preparation, additional experimental data, analysis, and discussion.

[40] E. H. Chowdhury, M. H. Rahman, S. Fatema, and M. M. Islam, Investigation of the mechanical properties and fracture mechanisms of graphene/WSe$_2$ vertical heterostructure: A molecular dynamics study, Comput. Mater. Sci. **188**, 110231 (2021).